J. Fluid Mech. (2003), *vol.* 497, *pp.* 365–380.
DOI: 10.1017/S0022112003006785 Printed in the United Kingdom

A mechanism for layer formation in a double-diffusive fluid

By TIMOUR RADKO

Department of Earth, Atmospheric and Planetary Sciences, Massachusetts Institute of Technology, 77 Massachusetts Avenue, Cambridge, MA 02139, USA

(Received 8 January 2003 and in revised form 12 August 2003)

The dynamics of layer formation by salt fingers from the uniform temperature and salinity gradients is studied by direct numerical simulations of the two-dimensional Navier–Stokes equations. It is shown that formation of steps in the model is caused by the parametric variation of the flux ratio ($\gamma = \overline{wT}/\overline{wS}$) as a function of the density ratio (R), which leads to an instability of equilibrium with uniform stratification. These unstable large-scale perturbations continuously grow in time until well-defined layers are formed. Subsequent evolution of the numerical staircases is explained by considering the secondary instabilities of a series of salt finger interfaces.

1. Introduction

One of the most dramatic signatures of active double-diffusion in the ocean is related to the formation of mixed layers separated by salt finger interfaces. Persistent staircases have been well documented in the Tyrrhenian Sea, below the Mediterranean outflow, and in the western tropical North Atlantic (Schmitt 1994). Layer formation is also observed in laboratory experiments (Stern & Turner 1969; Krishnamurti 2003).

Conventional explanations for the origin of thermohaline staircases include:

(i) collective instability (Stern 1969),

(ii) thermohaline intrusions which develop into a staircase (Merryfield 2000),

(iii) metastable equilibria, initially forced by the external disturbances (Stern & Turner 1969),

(iv) negative density diffusion (Schmitt 1994).

The applicability of these theories has been questioned in the literature, and the reader is referred to Merryfield (2000) who assessed the strengths and weaknesses of each hypothesis. Below, we briefly summarize some major difficulties in applying these ideas to the observations of layers in oceanic, experimental and numerical contexts.

Probably the most influential hypothesis for the formation of interfaces and layers involves collective instability, an effect in which salt fingers excite internal gravity waves when the Stern number $A = (\beta F_S - \alpha F_T)/(\nu(\alpha T_z - \beta S_z))$ exceeds a critical value of order unity. (F_T and F_S are the temperature and salinity fluxes; T_z and S_z are the vertical gradients; α, β are the expansion/contraction coefficients; ν is the molecular viscosity.) Stern (1969) suggested that the growing gravity wave might eventually overturn and generate a stepped structure. The measured values of A in

the oceanic staircases are indeed $O(1)$. However, in many laboratory experiments, salt and sugar replace the heat and salt as buoyancy components (e.g. Lambert & Demenkow 1972; Griffiths & Ruddick 1980), and Stern numbers there are extremely low. Lambert & Demenkow (1972) report values as low as $A = 2 \times 10^{-3}$, casting some doubt on the generality of Stern's (1969) criterion.

Thermohaline intrusions (hypothesis (ii)) necessarily require the presence of lateral $T - S$ gradients. Thus, while it can be argued that this effect may be relevant for some oceanic observations, it does not explain the formation of layers in a controlled laboratory setting and in numerical experiments where the $T - S$ gradients are exactly vertical. Formation of layers in the following numerical simulation occurs without external forcing, which suggests that the presence of external disturbances (hypothesis (iii)) also may not be essential.

In order to explain the formation and maintenance of layers, oceanographers often refer to the idea that the salt flux due to salt fingers exceeds the heat flux and therefore the buoyancy flux should be counter-gradient; this by itself would seem to favour growth of the perturbations on a uniform gradient (Schmitt 1994). It was suggested that unstable perturbations will eventually modify the background stratification, and form steps. This view may have some merit, but only in a very general and qualitative sense. Any meaningful quantitative model of double-diffusive layering should necessarily include the dynamics of both salt and heat. Schmitt (1981), followed by Walsh & Ruddick (1995), performed a stability analysis for double-diffusive stratified fluid using parameterized heat and salt fluxes. They concluded that, despite the counter-gradient flux of buoyancy, the uniform vertical $T - S$ gradient is stable, as long as the fluxes monotonically increase as the density ratio decreases. (The latter assumption has been confirmed by observations, laboratory experiments and numerical simulations; these are discussed in § 3.)

An important feature of the earlier stability theories (e.g. Schmitt 1981) was the assumption that the heat/salt flux ratio γ is independent of the density ratio R. This assumption simplifies the analytical development. However, it filters out an unstable mode, which, we argue, is essential for the formation and evolution of a thermohaline staircase. Dynamics and consequences of this instability (γ-instability hereinafter) is the focus of our study.

This paper is set out as follows. In § 2, we present a high-resolution numerical experiment, which demonstrates the ability of salt fingers to generate layers at low values of R. Layer formation is related to the γ-instability (§ 3) that occurs when the flux ratio is a decreasing function of R. Diagnostics of the direct numerical simulations (§ 4) show that the variable flux ratio plays a crucial role in the evolution of the large-scale $T - S$ fields in both linear and strongly nonlinear regimes. In § 5, we explore the dynamics and stability of the resulting thermohaline staircase. We summarize our conclusions in § 6.

2. Numerical simulations

Following Radko & Stern (1999), we consider the temperature and salinity fields, which consist of the linear basic state $(\bar{T}, \bar{S})$ and a departure (T, S) from it; periodic boundary conditions are assumed for the latter. Boussinesq equations are non-dimensionalized using the scales of the linearly fastest growing fingers: $d = (k_T \nu / g\alpha \bar{T}_z)^{1/4}$ is the unit of length; k_T/d is used as the velocity scale, d^2/k_T is the time scale, and $\alpha \bar{T}_z d$ is used as the scale for both temperature and salinity

perturbations, resulting in

$$\left.\begin{aligned} &\frac{1}{Pr}\frac{\mathrm{d}\boldsymbol{v}}{\mathrm{d}t} = -\nabla p + \nabla^2 \boldsymbol{v} + (T - S)\boldsymbol{k}, \\ &\nabla \cdot \boldsymbol{v} = 0, \\ &\frac{\mathrm{d}T}{\mathrm{d}t} + w = \nabla^2 T, \\ &\frac{\mathrm{d}S}{\mathrm{d}t} + \frac{1}{R_0} w = \tau \nabla^2 S, \end{aligned}\right\} \tag{1}$$

where $Pr = \nu/k_T$ is the Prandtl number, $\tau = k_S/k_T$ is the molecular diffusivity ratio (Lewis number), and R_0 is the density ratio for the basic uniform $T - S$ gradient. The influence of the underlying uniform gradients appears in the coefficients of w.

The system of equations in (1) is solved numerically in two dimensions using a fully dealiased pseudospectral method described and first used in Stern & Radko (1998). In the following calculation, we use a diffusivity ratio of $\tau = 1/3$ which is higher than the heat/salt value ($\tau = 1/100$). This choice is dictated by numerical convenience – otherwise it becomes necessary to resolve salt filaments on the scales which are much less than the characteristic finger width. Nevertheless, as argued in Stern, Radko & Simeonov (2001), such a modification is not expected to alter the fundamental physics and dynamics of salt fingering. Since the observations (e.g. Schmitt 1981) suggest that layers tend to form at low values of the density ratio, we use $R_0 = 1.1$, and the Prandtl number is $Pr = 7$. The size of the computational domain is $L = 335$ in x and $H = 536$ in z, which corresponds to (25×40) fastest growing, on the original gradient, finger wavelengths (FGW hereinafter). The flow is resolved by a uniform mesh with $(N_x \times N_z) = (512 \times 512)$ elements, and the model is initialized from rest by a small-amplitude random computer-generated initial (T, S) distribution.

After a few characteristic growth periods, active double-diffusive convection is established ($t \sim 10$). The time scale associated with formation of the staircase is, however, much larger. Thus, figure 1(*a*) shows the instantaneous temperature field at $t = 50$, which exhibits typical signatures (e.g. Stern *et al.* 2001) of a fully developed chaotic field of two-dimensional salt fingers, but no visible signs of layer formation. Figure 1(*b*) illustrates the dramatic change in the pattern of the temperature field at $t = 400$ associated with the appearance of the well-defined horizontal layers. These layers are not steady, but evolve further in time. Their number continuously decreases and the characteristic vertical scale of layers correspondingly increases until there is only one layer left within the limits of our computational domain ($t = 800$ in figure 1*c*).

Modification of vertical stratification by double diffusion is shown in figure 2, in which we plot the total horizontally averaged density

$$\bar{\rho}_{total} = (1 - R^{-1})z + \sigma - \theta,$$

where $\theta(z)$ and $\sigma(z)$ are the horizontal averages of T and S, respectively. The well-defined steps in figure 2(*b–f*) consist of nearly uniform layers separated by thin stratified interfaces. In time, the mixed layers merge, thereby eliminating some interfaces.

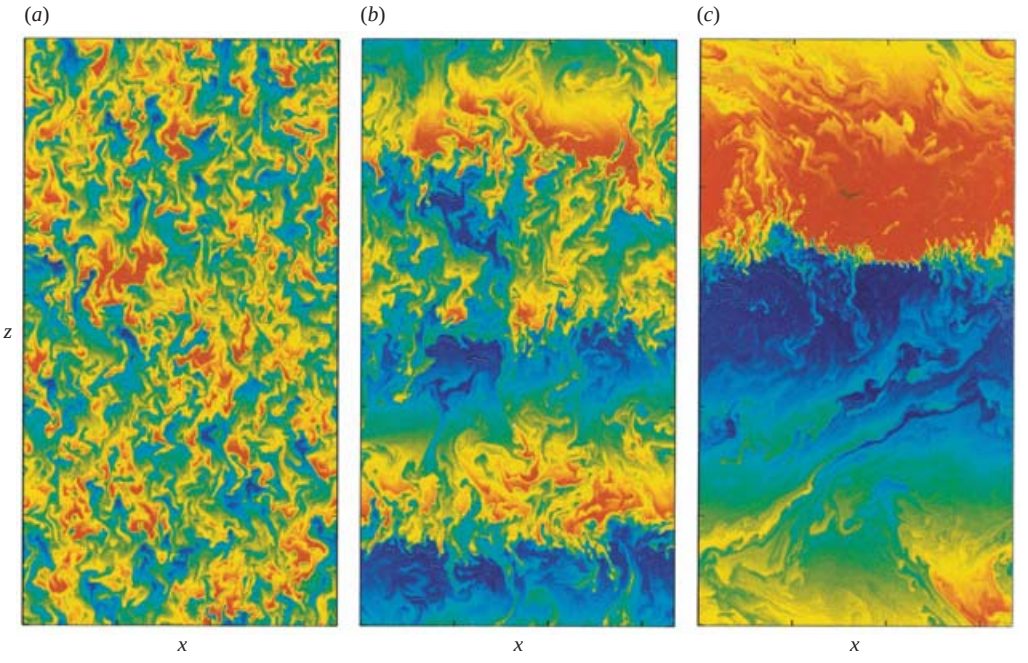

FIGURE 1. Formation and evolution of layers in the numerical experiment. Instantaneous temperature fields are shown for (*a*) $t = 50$, (*b*) $t = 400$ and (*c*) $t = 800$. Red colour corresponds to high values of T, and low values are shown in blue.

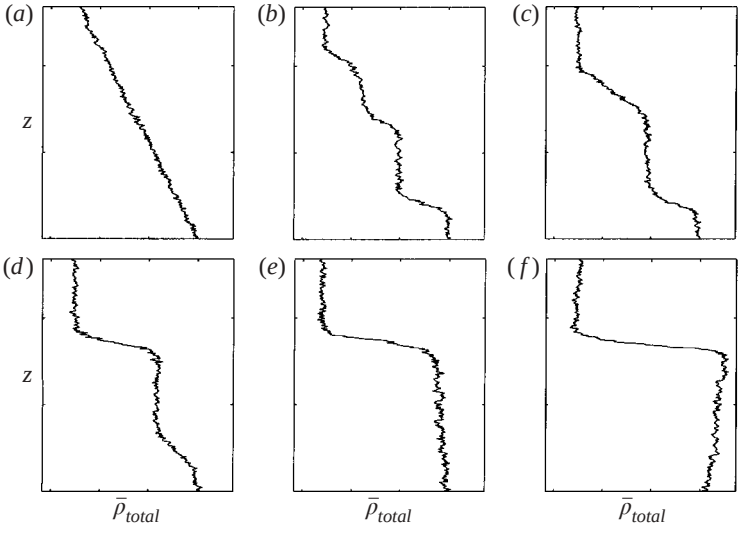

FIGURE 2. The total x-averaged density for the calculation in figure 1 at (*a*)–(*f*) $t = 100$, 400, 500, 600, 700, 800. Note the appearance, by $t = 400$, of nearly homogeneous layers separated by thin stratified interfaces, and their subsequent merger.

3. Instability of the gradient flux laws

In this section, we develop a theoretical framework for the interaction of fingers with the larger scales of motion.† In order to represent large-scale effects of a stochastic field of fingers, we average the $T-S$ equation in (1) over spatial/time scales that greatly exceed those for individual salt fingers. Guided by the foregoing numerical results, we focus on one-dimensional effects and assume that averaged quantities depend only on z and t (the individual fingers could be either two- or three-dimensional). The resulting large-scale $T-S$ equations are

$$\frac{\partial T_f}{\partial t} = -\frac{\partial}{\partial z} F_T, \quad \frac{\partial S_f}{\partial t} = -\frac{\partial}{\partial z} F_S, \tag{2}$$

where $T_f = \langle T \rangle$, $S_f = \langle S \rangle$ are the averaged temperature and salinity fields, $F_T = \langle wT \rangle - \partial \langle T \rangle / \partial z$, $F_S = \langle wS \rangle - \tau \partial \langle S \rangle / \partial z$, and averaging is denoted by the angular brackets. Although small molecular fluxes in (F_T, F_S) could be retained in the following theory, we prefer to simplify the argument by considering only the dominant contribution from salt fingering.

Following Stern *et al.* (2001), we assume that the averaged (non-dimensionalized) fluxes depend on local large-scale gradients. Thus,

$$F_T = -Nu \frac{\partial T_{f\,total}}{\partial z}, \quad F_S = \frac{1}{\gamma} F_T, \tag{3}$$

where $T_{f\,total} = z + T_f$ is the total large-scale temperature field, which includes both the uniform basic gradient and its local modification ($T_f(z)$), $S_{f\,total}$ is the total salinity field. Parameters γ and $Nu > 0$ in (3) are the flux ratio and the Nusselt number (ratio of the local salt finger and molecular heat fluxes). If the $T-S$ fluxes depend only on the local gradients, then it can be argued on dimensional grounds that both γ and Nu are determined by the local density ratio

$$R = \frac{(\partial/\partial z) T_{f\,total}}{(\partial/\partial z) S_{f\,total}} = \frac{1 + (\partial/\partial z) T_f}{1/R_0 + (\partial/\partial z) S_f}. \tag{4}$$

Qualitative behaviour of $\gamma(R)$ and $Nu(R)$ is indicated in the schematic diagram in figure 3. $Nu(R)$ is a decreasing function of R, reflecting the tendency of double-diffusion to intensify as we move away from the marginal instability point ($R = 1/\tau$). This prediction is supported by the numerous laboratory (Wells & Griffiths 2002), observational (St Laurent & Schmitt 1999), and numerical (Stern *et al.* 2001) evidence.

The flux ratio $\gamma(R)$ is, however, non-monotonic (figure 3). As R is decreased from $1/\tau$, $\gamma(R)$ first decreases, reaches its minimum value at a point (R_{min}) in the interior of the salt finger interval $1 < R_{min} < 1/\tau$, and then increases. This feature occurs in both salt–sugar and heat–salt experiments, and can be rationalized (Schmitt 1979) by considering fluxes in the linearly fastest growing fingers. Schmitt's model suggests $R_{min} \sim 1.3$ for sugar/salt fingers and $R_{min} \sim 4$ for heat and salt; this theory is also qualitatively supported by the numerical, laboratory and field experiments (e.g. St Laurent & Schmitt 1999).

Consider the relatively weak perturbations of the basic uniform gradient that are characterized by $\partial T_f/\partial z$, $\partial S_f/\partial z \ll 1$, and then linearize (4), neglecting the terms of

† An anonymous referee pointed out that the following analytical solution can be considered as a particular case of the intrusion theory in Walsh & Ruddick (2000) in the limit of vanishing horizontal gradients. However, this case is essential for interpretation of our numerical simulations, and a full discussion of the γ-instability is included herein.

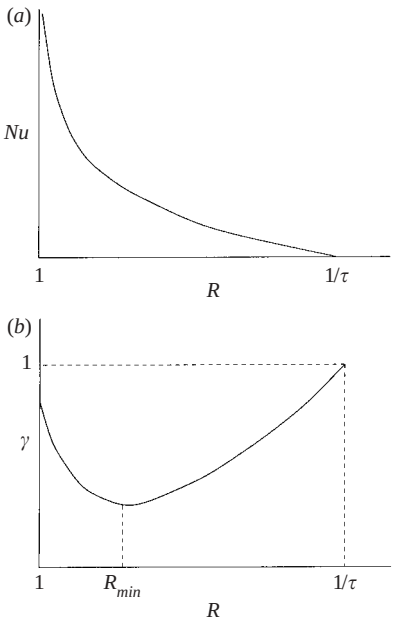

FIGURE 3. Dependence of (a) the Nusselt number Nu and (b) the flux ratio γ on the density ratio R.

the order $(\partial T_f/\partial z)^2$:

$$R = R_0 + R_0\left(\frac{\partial T_f}{\partial z} - R_0\frac{\partial S_f}{\partial z}\right) + \ldots. \tag{5}$$

Next, we substitute (3) into (2) and linearize the result, retaining only the $[O(\partial^2 T_f/\partial z^2)]$ terms:

$$\left.\begin{aligned} \frac{\partial T_f}{\partial t} &= \left.\frac{\partial Nu}{\partial R}\right|_{R=R_0}\frac{\partial R}{\partial z} + Nu(R_0)\frac{\partial^2 T_f}{\partial z^2}, \\ \frac{\partial S_f}{\partial t} &= \left.\frac{\partial \gamma^{-1}}{\partial R}\right|_{R=R_0}\frac{\partial R}{\partial z}Nu(R_0) + \gamma^{-1}(R_0)\frac{\partial T_f}{\partial t}. \end{aligned}\right\} \tag{6}$$

In order to analyse the stability of the linear system in (5) and (6), we consider the normal modes $(T_f, S_f) = (\hat{T}, \hat{S})\exp(\lambda t)\sin(kz)$, which reduce it to:

$$\left.\begin{aligned} \lambda\hat{T} &= -k^2[A_2(\hat{T} - R_0\hat{S}) + Nu(R_0)\hat{T}], \\ \lambda(\hat{S} - (1/\gamma(R_0))\hat{T}) &= -k^2[Nu(R_0)A_1(\hat{T} - R_0\hat{S})], \end{aligned}\right\} \tag{7}$$

where

$$A_1 = \left.\frac{\partial(1/\gamma)}{\partial R}\right|_{R=R_0} R_0, \tag{8}$$

and

$$A_2 = \left.\frac{\partial Nu}{\partial R}\right|_{R=R_0} R_0. \tag{9}$$

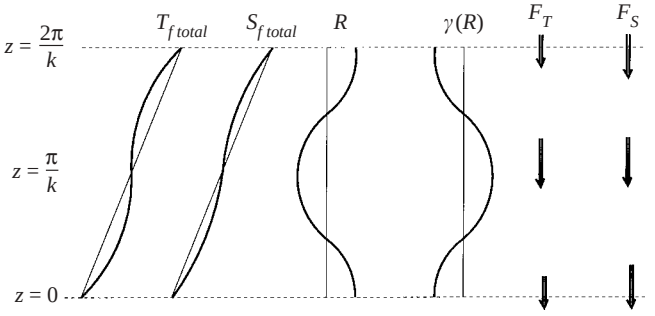

FIGURE 4. Schematic diagram illustrating the physical mechanism of the γ-instability. Decrease in γ with R results in the growth of the perturbations on a uniform $T - S$ gradient (see the text).

When $\hat{T}$ and $\hat{S}$ are eliminated in (7), we arrive at the quadratic eigenvalue equation for the growth rate λ:

$$\lambda^2 + \lambda\left(A_2 + Nu(R_0) - A_1 Nu(R_0)R_0 - \frac{R_0 A_2}{\gamma(R_0)}\right)k^2 - A_1 Nu^2(R_0)R_0 k^4 = 0. \qquad (10)$$

Consider sufficiently small values of the density ratio in the interval $1 < R_0 < R_{min}$ for which $\gamma(R)$ decreases with R (see figure 3) and therefore $A_1 > 0$. Since the free coefficient of the quadratic equation (10) is negative in this range, there are two real roots ($\lambda_1 > \lambda_2$) of opposite sign. The existence of a positive root (λ_1) implies the instability of the basic uniform gradient.

Analysis of the amplitude/phase relationships for T, S, R and γ in a growing normal mode suggests the following physical explanation of layering instability. If the amplitude of the temperature perturbation ($\hat{T}$) exceeds the amplitude of the salt perturbation ($\hat{S}$), as shown in a schematic diagram in figure 4, then the density ratio R reaches its maximum at the location of the largest temperature gradient (that is $z = 0$ in figure 4). As is clear from (3), the heat flux is affected by both the local gradient ($\partial T_{f\,total}/\partial z$) and the density ratio through $Nu(R)$, and these processes act in the opposite sense. If γ were constant, then, for the first normal mode in (7) and (10), these two effects would exactly compensate for each other; F_T would be independent of z and, in the absence of vertical convergence, the temperature amplitude would not change in time. When γ is a decreasing function of R, there will be an increase of the heat/salt flux ratio at $z = \pi/k$ and, correspondingly, a decrease at $z = 0, 2\pi/k$. As a result, the temperature flux convergence at $0 < z < \pi/k$ (and divergence at $\pi/k < z < 2\pi/k$) exceeds that for salt. This convergence pattern leads to an enhanced accumulation of heat, relative to the accumulation of salt, in the lower part of the layer in figure 4. This, in turn, is followed by an additional increase in the amplitude of $R - R_0$ at $z = 0$ and, correspondingly, further decreases γ at $z = 0$. This self-enhancing mechanism produces a monotonic growth of the perturbation which, we argue, eventually leads to the formation of well-defined layers and interfaces.

We now make a crude estimate of the growth rate of this layering instability for the oceanic (heat/salt) parameters. Calculations in Stern *et al.* (2001) suggest that for $R_0 < 2$, $Nu \sim 10^2$, $\partial Nu/\partial R \sim -10^2$, $\gamma \sim 0.7$, $\partial\gamma/\partial R \sim -10^{-1}$, and hence $A_2 \sim -10^2$, $A_1 \sim 0.1$. For $A_1 \ll 1$, the expressions for the roots of the quadratic equation (8) reduce

to a simple approximate form:

$$\left.\begin{aligned}\lambda_1 &= \frac{A_1 Nu^2(R_0) R_0 k^2}{Nu(R_0) - A_2(\gamma^{-1}(R_0)R_0 - 1)} > 0,\\ \lambda_2 &= (A_2(\gamma^{-1}(R_0)R_0 - 1) - Nu(R_0))k^2 < 0.\end{aligned}\right\} \tag{11}$$

Substituting the above scales in (11), we estimate $\lambda_1 \sim 10k^2$. In dimensional units, this corresponds to an e-folding period of $t_{dim} \sim H_{dim}^2/40\pi^2 k_T$, where H_{dim} is the (dimensional) vertical wavelength. Thus, for fixed R, the characteristic layering period scales, relative to the fingering timescale, as a square of the ratio of the layer height to the fastest-growing finger width. For scales of $H_{dim} \sim (1\text{–}10)\,\mathrm{m}$ and $k_T \sim 10^{-7}\mathrm{m}^2\,\mathrm{s}^{-1}$, the characteristic layering time is in the range of 8 hours to a month. Given the persistence of oceanic thermohaline staircases over 25 years or more (Schmitt 1994), it is clear that there is more than enough time for our instability to modify a smooth gradient and establish well-defined steps.

Note that (11) implies the increase of the growth rate as the wavenumber of the disturbances increases. (Of course, the theory itself is valid only for scales that exceed the characteristic salt finger width.) This ultraviolet catastrophe in our model is consistent with the pattern of layer formation in numerical experiments (figure 2), which show that the layers formed first are very thin, only a few salt fingers in height.

Before we proceed to examine the role of the γ-instability in the numerical layer formation, it is of interest to note that many earlier theories for salt fingers based on the parameterized gradient flux laws (e.g. Schmitt 1981; Walsh & Ruddick 1995; Stern *et al.* 2001) assumed, for reasons of tractability, that γ is constant (i.e. $A_1 = 0$). As shown above, this approximation sets λ_1 to zero and thereby filters out the layering mode of instability.

4. Comparison of theory with direct numerical simulations

To show that staircase formation in the foregoing (§ 2) experiments is related to the γ-instability mechanism (§ 3), we now present supporting diagnostics of the direct numerical simulations. In § 4.1, we test the linear instability theory, and in § 4.2, we diagnose the balances in the potential energy budget for the fully nonlinear calculation.

4.1. *Linear instability*

In order to use quantitatively the linear theory in § 3, we have to know the derivatives of the Nusselt number and flux ratio (A_1 and A_2) at $R_0 = 1.1$. These numbers were estimated by performing two experiments for $R_1 = 1.075$ and $R_2 = 1.125$. In both cases we used computational domains that correspond to (6×20) FGW resolved by (128×512) elements. The models were initiated using a random (T, S) initial distribution and integrated for 100 units of time during which no layers formed. Heat fluxes and flux ratios reached a quasi-equilibrium level of

$$Nu(R_1) = 147, \quad \gamma(R_1) = 0.8547, \quad R_1 = 1.075, \tag{12}$$

$$Nu(R_2) = 112, \quad \gamma(R_2) = 0.8478, \quad R_2 = 1.125. \tag{13}$$

Using these gradient fluxes, we estimate the terms in (8) and (9) to be $A_1 = 0.21$ and $A_2 = -770$, and $Nu(R_0) = 130$ ($R_0 = 1.1$). For the growing large-scale normal mode,

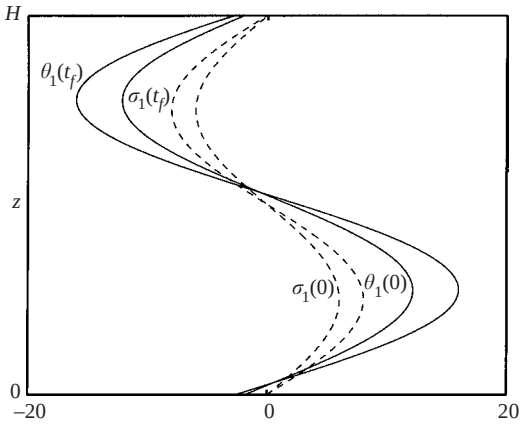

FIGURE 5. Evolution of the normal mode in the direct numerical simulation. The horizontally averaged $T-S$ fields are Fourier analysed and the fundamental harmonics (θ_1, σ_1) are plotted. Solid (dashed) lines correspond to the final (initial) state. Growth rate and amplitude/phase relationships are consistent with theoretical prediction.

equations (7) and (10) then yield the amplitude ratio of

$$\frac{\hat{T}}{\hat{S}} = 1.34, \tag{14}$$

and the growth rate

$$\lambda = \frac{456}{H^2}, \tag{15}$$

where H is a z-wavelength.

To test how well our linear theory is realized in direct numerical simulations, our next experiment was initiated using the small-amplitude unstable normal mode of fundamental wavelength. As above, the computational domain corresponded to (6×20) FGW resolved by (128×512) mesh. For $R_0 = 1.1$, the height of the domain is $H = 268$, and therefore from (15) the expected growth rate is

$$\lambda_{theor} = 0.0063. \tag{16}$$

In addition to the normal mode shown by dashed lines in figure 5, random noise (at the level of $\sim 5\%$ of the normal mode) was also initially introduced to expedite the development of fingers. The model was integrated for 100 time units, and the final x-averaged temperature and salinity fields (θ, σ) were Fourier analysed in z. The fundamental harmonic (θ_1, σ_1) at $t_f = 100$ is shown in figure 5 by solid lines.

The predicted zero spatial phase lag between temperature and salinity modes is apparently preserved in the numerical simulation, as is the theoretical amplitude ratio (14). The ratio of the amplitudes of θ_1 at $t = 0$ and $t_f = 100$ in figure 5 implies the growth rate of

$$\lambda_{num} = 0.0069,$$

which agrees well with the theoretical prediction (16), given all the approximations involved in the analytical theory in § 3. Thus, our analysis proves that the analytical solution is realizable in the sense of an initial-value calculation. However, it remains to be shown that modification of the basic gradient for the complex and unbiased initial conditions is also caused by the γ-instability. This will be demonstrated below.

4.2. *Integral balances*

To quantify the role of the γ-instability in the growth of large-scale perturbations in the experiment in figure 1, we first x-average the governing $T-S$ equations (1) resulting in

$$\frac{\partial\theta}{\partial t}+\frac{\partial\overline{wT}}{\partial z}=\frac{\partial^2\theta}{\partial z^2},\quad \frac{\partial\sigma}{\partial t}+\frac{\partial\overline{wS}}{\partial z}=\tau\frac{\partial^2\sigma}{\partial z^2}, \tag{17}$$

where $(\theta,\sigma,\overline{wT},\overline{wS})$ are the horizontal averages of (T,S,wT,wS). Next, we average (17) in z over a scale that exceeds the characteristic size of the salt fingers. In our diagnostic calculations this is done by Fourier analysing (17) in z and retaining only the 5 lowest harmonics. In addition, equations of motion are also smoothed in time, which is implemented in the numerics by computing (online) the running average of terms in (17) with an averaging interval of Δt=25. The resulting large spatial/time scale equations are:

$$\frac{\partial\theta_f}{\partial t}+\frac{\partial F^*_{Tf}}{\partial z}=0,\quad \frac{\partial\sigma_f}{\partial t}+\frac{\partial F^*_{Sf}}{\partial z}=0, \tag{18}$$

where

$$F^*_{Tf}=(\overline{wT})_f-\frac{\partial\theta_f}{\partial z},\quad F^*_{Sf}=(\overline{wS})_f-\tau\frac{\partial\sigma_f}{\partial z}.$$

Subscript f in (18) pertains to the averaged quantities, and the fluxes include the small contributions from molecular diffusion, denoted by asterisks. Subtracting the two equations in (18) we obtain the density equation:

$$\frac{\partial\rho_f}{\partial t}+\frac{\partial F^*_{Sf}}{\partial z}-\frac{\partial F^*_{Tf}}{\partial z}=0, \tag{19}$$

where $\rho_f=\sigma_f-\theta_f$. The integral equation for the density variance (i.e. perturbation potential energy) is obtained by multiplying (19) by ρ_f and integrating in z over the extent of the computational domain. After some rearranging, the density variance equation becomes:

$$\frac{\partial}{\partial t}\int\frac{\rho_f^2}{2}\,\mathrm{d}z=\int\rho_f\left[1-\frac{F^*_{Sf}}{F^*_{Tf}}\right]\frac{\partial}{\partial z}F^*_{Tf}\,\mathrm{d}z+\int\rho_f F^*_{Tf}\frac{\partial}{\partial z}\left[-\frac{F^*_{Sf}}{F^*_{Tf}}\right]\mathrm{d}z. \tag{20}$$

Equation (20) is one of the key elements of our model. The growth of the density variance is associated with destruction of the uniform stratification (for which the density variance is identically zero) and formation of steps, and therefore partitioning of terms in (20) may determine the cause of layering. The first term on the right-hand side of (20) represents the processes that occur because of the variation in the heat flux, while the second is related to the variation in the flux ratio. These integrals (I_{Nu} and I_γ hereinafter) were continuously recorded in the course of the numerical experiment in § 2, and the results are in figure 6. Since our major objective is to explain the onset of layering, we first examine (figure 6*a*) the evolution of I_{Nu} and I_γ during the period of layer formation, before the first density overturns. Figure 6(*a*) indicates that the growth of the large-scale perturbation is associated with the variation in γ. I_{Nu} acts in the opposite sense, tending to decrease density variance and restore uniformity of the stratification.

The quasi-monotonic growth of I_γ and I_{Nu} in the first stage of the experiment ($t<300$) changes to a more irregular pattern after formation of the convective layers; these terms start to oscillate vigorously and occasionally change sign. Nevertheless, on average, it is still the I_γ term that causes the growth of density variance, and I_{Nu} has

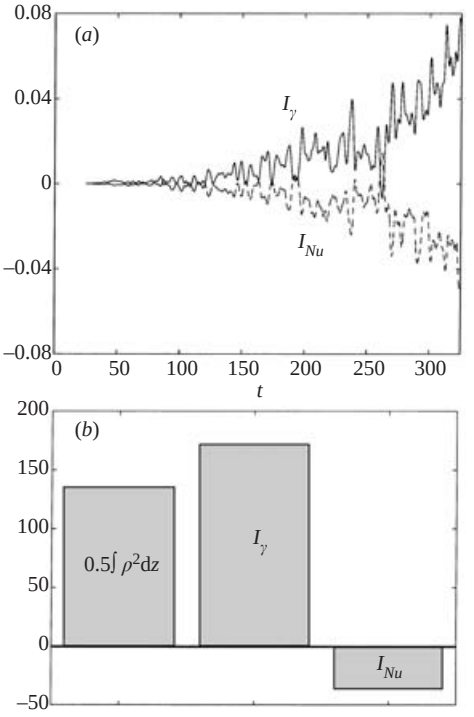

FIGURE 6. Balance of terms in the density variance equation (20). (*a*) Time evolution of the term associated with variation in γ (variation in Nu) is shown by solid (dashed) line for the period of layer formation ($t < 300$) (*b*) Integral contribution of I_γ and I_{Nu} during the experiment in figures 1 and 2. Increase in the density variance is caused by the γ-effect (see the text).

an adverse overall effect. To quantify the integral contributions of the two processes over the duration of the experiment in figure 1, the density variance equation is integrated in time:

$$\int \frac{\rho_f^2}{2}\,\mathrm{d}z\bigg|_{final} = \int I_{Nu}\,\mathrm{d}t + \int I_\gamma\,\mathrm{d}t. \tag{21}$$

Partitioning of the terms in (21), diagnosed from the numerics, is shown in the histogram in figure 6(*b*). We see that the density variance is produced by the γ-instability. On the other hand, variation in the Nusselt number, which causes the collective instability (see Stern *et al.* 2001), has a weak negative effect in our experiment.

Of course, conjectures based on (20) implicitly assume that the density is more fundamental dynamically than, say, salinity or temperature alone. Although this assumption is plausible and rather conventional, it must be demonstrated rather than postulated. Nevertheless, we consider the diagnostics in figure 6 suggestive, since they reveal the significance of the variable flux ratio in the formation and evolution of the thermohaline staircase.

5. Instability of a series of interfaces

What happens after layers develop? Numerical calculations (§ 2) suggest that the layers formed initially are not steady but evolve further. There is a general tendency

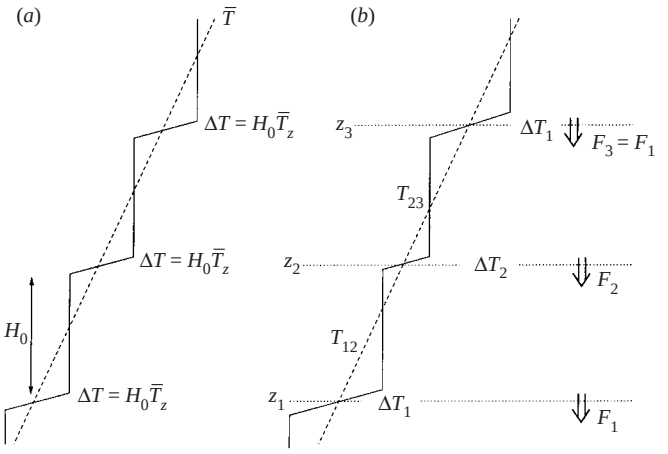

FIGURE 7. Schematic diagram illustrating the stability analysis for an infinite series of interfaces. (*a*) Basic state consisting of identical steps. (*b*) Perturbed state in which the $T - S$ jumps at the even interfaces are slightly decreased, and the jumps at odd interfaces are increased correspondingly.

for the strong steps characterized by significant temperature and salinity jumps (ΔT, ΔS) to grow further at the expense of weaker steps; the latter gradually erode and eventually disappear. As a result, the number of steps decreases in time, and by the end of the calculation in figure 2 there is only one interface left within the limits of the computational domain. To explain the observed layer interactions, we now consider the stability of a series of salt finger interfaces. The solution technique is analogous to that used by Huppert (1971) who discussed stability of diffusive interfaces; in our case, it is also modified to describe the periodic system used in the numerics (§ 2).

The schematic diagram in figure 7(*a*) shows a basic state consisting of a series of identical thin interfaces separated by mixed layers of equal thickness (H_0). We now perturb this equilibrium state in a way indicated in figure 7(*b*). We slightly increase the $T - S$ jump at the interface $z = z_1$, but decrease the jump at neighbouring interfaces by exactly the same amount; the vertical structure is assumed to be periodic with the z-wavelength of $2H_0$. Thus, the state in figure 7 can be thought of as an infinite series of layers in which we simultaneously reduced the magnitude of (ΔT, ΔS) at all the interfaces with even numbers and correspondingly increased the $T - S$ jumps across the odd interfaces. Note that such a perturbation does not affect the overall $T - S$ gradient. The objective is to determine whether the disturbance can grow in time, implying instability of the basic state in figure 7, or remain small.

For the purpose of this section it is convenient to present the theory in dimensional units. To be specific, we use the conventional 4/3 flux law (Turner 1967) for the downward flux across the interfaces, which can be written as

$$\beta F_{S\,dim} = C_S(R)(\beta \Delta S_{dim})^{4/3}. \tag{22}$$

The 4/3 flux law can be formally derived using dimensional arguments, and detailed physical models (e.g. Radko & Stern 2000) have been developed to explain the dynamical effects leading to (22). It should be mentioned, however, that the stability/instability of our system does not depend on the specific flux law, and different formulations would yield the same results as long as F_S increases with ΔS. For convenience,

we rewrite (22) in the following equivalent form:

$$F_T = C(R)(\Delta T)^{4/3}, \quad F_S = \frac{1}{\gamma(R)} F_T, \tag{23}$$

where the expansion/contraction coefficients (α, β) are now absorbed in (T, S), and $\gamma(R)$ is a flux ratio.

In time, $(\Delta T, \Delta S)$ across an interface can change, as well as the distance between neighbouring interfaces. While both effects are realized in the oceanic and laboratory contexts, the vertical drift of the salt finger interface is usually (e.g. McDougall 1991) related to the nonlinearity of the equation of state, and therefore it is beyond the scope of the present model. In addition, the foregoing numerical experiments indicate that the evolution of interfaces in time is associated mostly with variation in $(\Delta T, \Delta S)$ and not with their vertical drift. Thus, the distance between neighbouring interfaces H_0 is assumed constant, and the rate of change of mixed-layer temperatures for a set-up in figure 7 is then simply

$$H_0 \frac{\partial}{\partial t} T_{12} = F_{T2} - F_{T1}, \quad H_0 \frac{\partial}{\partial t} T_{23} = F_{T3} - F_{T2}, \ldots, \tag{24}$$

where $T_{n\,n+1}$ is the temperature of the mixed layer bounded by interfaces n and $n+1$, so that $\Delta T_n = T_{n\,n+1} - T_{n-1\,n}$. The assumed periodicity of the staircase in figure 7 implies that

$$\Delta T_1 + \Delta T_2 = 2H_0 \frac{\partial \bar{T}}{\partial z}, \tag{25}$$

$$F_{T1} = F_{T3}, \tag{26}$$

where $\partial \bar{T}/\partial z$ is the overall temperature gradient. Next, we subtract the two equations in (24) and simplify the result using (25):

$$H_0 \frac{\partial}{\partial t}(\Delta T_1) = 2(F_{T2} - F_{T1}).$$

The flux law (23) reduces this expression to

$$H_0 \frac{\partial}{\partial t}(\Delta T_1) = 2C(R_2)(\Delta T_2)^{4/3} - 2C(R_1)(\Delta T_1)^{4/3}, \tag{27}$$

where $R_i = \Delta T_i / \Delta S_i$, and the corresponding salinity equation is:

$$H_0 \frac{\partial}{\partial t}(\Delta S_1) = 2\frac{C(R_2)}{\gamma(R_2)}(\Delta T_2)^{4/3} - 2\frac{C(R_1)}{\gamma(R_1)}(\Delta T_1)^{4/3}. \tag{28}$$

We now simplify our key relations by introducing the following variables

$$A = \frac{\Delta T_1 - H_0 \bar{T}_z}{H_0 \bar{T}_z}, \quad B = \frac{\Delta S_1 - H_0 \bar{S}_z}{H_0 \bar{S}_z},$$

which represent the relative increase in the magnitude of interfacial jumps in the perturbed state with respect to their equilibrium values. Accordingly,

$$\Delta T_1 = (1 + A) H_0 \frac{\partial \bar{T}}{\partial z}, \quad \Delta T_2 = (1 - A) H_0 \frac{\partial \bar{T}}{\partial z},$$

$$\Delta S_1 = (1 + B) H_0 \frac{\partial \bar{S}}{\partial z}, \quad \Delta S_2 = (1 - B) H_0 \frac{\partial \bar{S}}{\partial z}.$$

When these are used in (27) and (28), we arrive at a closed system of ordinary differential equations for A and B:

$$\left.\begin{aligned}
&\frac{\partial A}{\partial t} = G\big(C(R_2)(1-A)^{4/3} - C(R_1)(1+A)^{4/3}\big),\\
&\frac{\partial B}{\partial t}\frac{1}{\bar{R}} = G\left(\frac{C(R_2)}{\gamma(R_2)}(1-A)^{4/3} - \frac{C(R_1)}{\gamma(R_1)}(1+A)^{4/3}\right),\\
&R_1 = \frac{1+A}{1+B}\bar{R},\\
&R_2 = \frac{1-A}{1-B}\bar{R},
\end{aligned}\right\} \tag{29}$$

where $G = 2(\bar{T}_z)^{1/3}/H_0^{2/3}$, and $\bar{R} = \bar{T}_z/\bar{S}_z$ is the density ratio in undisturbed interfaces. Qualitative behaviour of $C(R)$ and $\gamma(R)$ for salt finger interfaces sandwiched between mixed layers is known from the laboratory experiments (e.g. Griffiths & Ruddick 1980) and theoretical models (Radko & Stern 2000); $C(R)$ is a decreasing function of R, whereas $\gamma(R)$ follows the pattern shown in figure 3 . As previously, we focus our discussion on the sufficiently low values of R, for which $\partial\gamma/\partial R < 0$.

In order to analyse the stability of the basic state, we consider $A, B \ll 1$ and linearize (29) using:

$$\begin{aligned}
R_1 &= \bar{R}(1+A-B) + \ldots,\\
R_2 &= \bar{R}(1-A+B) + \ldots,\\
\frac{1}{\gamma(R_1)} &= \frac{1}{\gamma(\bar{R})} + D_1(A-B) + \ldots,\\
\frac{1}{\gamma(R_2)} &= \frac{1}{\gamma(\bar{R})} + D_1(B-A) + \ldots,\\
C(R_1) &= C(\bar{R}) + D_2(A-B) + \ldots,
\end{aligned}$$

where

$$D_1 = \left.\frac{\partial(1/\gamma)}{\partial R}\right|_{R=\bar{R}} \bar{R} > 0, \quad D_2 = \left.\frac{\partial C}{\partial R}\right|_{R=\bar{R}} \bar{R} < 0.$$

The resulting linearized system for (A, B) is

$$\left.\begin{aligned}
&\frac{\partial A}{\partial t} = 2G[D_2(B-A) - 4/3C(\bar{R})A],\\
&\frac{\partial B}{\partial t}\frac{1}{\bar{R}} = 2G\left[\frac{D_2}{\gamma(\bar{R})}(B-A) + C(\bar{R})D_1(B-A) - 4/3\frac{C(\bar{R})}{\gamma(\bar{R})}A\right].
\end{aligned}\right\} \tag{30}$$

Substitution of normal modes $(A, B) = (A_0, B_0)\exp(\lambda t)$ in (30) yields the eigenvalue equation for growth rates:

$$\lambda^2 + 2G\left[4/3C(\bar{R}) + D_2 - \frac{\bar{R}D_2}{\gamma(\bar{R})} - D_1C(\bar{R})\bar{R}\right]\lambda - 16/3G^2C(\bar{R})^2D_1\bar{R} = 0. \tag{31}$$

For $D_1 > 0$, this quadratic equation has two real roots of opposite sign. Existence of a positive eigenvalue implies instability of the basic field, suggesting that 'strong' interfaces, characterized by larger $(\Delta T, \Delta S)$, should grow at the expense of weaker interfaces.

Since the foregoing linear analysis is not formally valid when the strengths of neighbouring interfaces are significantly different, we also performed numerical integrations

of the fully nonlinear equations in (29). Simple and qualitatively plausible empirical functions have been used for $C(R)$ and $\gamma(R)$. These calculations (not shown) suggested that unstable perturbations do not equilibrate at finite amplitude, but grow continuously, resulting in the complete destruction of a weaker interface. Thus, this instability mechanism explains the coarsening of layers observed in the direct numerical simulations (cf. figure 2). It is important to emphasize that merging of layers in the foregoing theory is also caused by the γ-effect – decrease of the flux ratio with density ratio at low values of R.

6. Discussion

This paper presents numerical and theoretical models of layer formation and evolution in a salt-fingering favourable fluid. Linear stability analysis shows that the uniform temperature–salinity gradient is unstable as long as the flux ratio (γ) is a decreasing function of the density ratio (R). The instability manifests itself in the form of growing, horizontally uniform perturbations, which eventually transform the basic gradient into a stepped structure consisting of salt finger interfaces sandwiched between the nearly homogeneous layers. The significance of the γ-effect for (numerical) layering was demonstrated by (i) testing linear instability theory *vs.* direct numerical simulations and (ii) diagnosing an integral balance based on the density variance equation. Both diagnostics suggest that layer formation is directly linked to variations in the flux ratio. Layers that initially develop in our simulations are not steady but merge continuously, which is also shown to be a consequence of the variable γ in our model. The characteristic height of steps increases in time until reaching the maximum scale resolved by the computational grid. Oceanic observations, however, suggest the existence of a finite vertical scale for the thermohaline steps. What arrests the coarsening of layers and thereby sets the vertical scale of steps in the oceanic staircases is an important question, which should be addressed in the future.

In connection with possible oceanographic applications of our model, we would like to mention that the pattern of $\gamma(R)$ for the oceanic (heat/salt) parameters is such that the most significant decrease in γ with R occurs within the interval $1 < R < 2$ (see figure 10 in St Laurent & Schmitt 1999, or figure 3 in Kunze 2003). Therefore, the γ-instability and resulting layering is expected for $R < 2$. This prediction is consistent with oceanic observations (Schmitt 1981) which indicate that pronounced staircases usually form in the regions where the density ratio is sufficiently low, as in the Tyrrhenian Sea ($R \sim 1.15$), Mediterranean outflow ($R \sim 1.3$), or Subtropical Underwater in the Caribbean ($R \sim 1.6$). No examples of staircase layering have been reported for $R > 2$. Thus, among the various layering mechanisms discussed in § 1 the γ-instability theory is particularly suggestive in relating the formation of layers to the environmental conditions. Likewise, recent careful laboratory experiments with the sugar/salt solute (Krishnamurti 2003) revealed spontaneous layer formation from the uniform gradient for $R \leqslant 1.25$. This result is also consistent with our theory since for the sugar/salt parameters $R_{min} = 1.3$, according to the fastest growing finger model in Schmitt (1979).

While this paper is focused on the salt-fingering case, it is straightforward to reinterpret all our analytical arguments for diffusive convection – cold fresh fluid above hot and salty. It remains to be determined how well the theoretical predictions are realized in the direct numerical simulations of the diffusive interface. Finally, note that many features of double-diffusive layering are very similar to those for turbulent one-component fluids (Balmforth *et al.* 1998); these include the formation

of thin layers as a result of the flux law instabilities and their subsequent coarsening. However, the coarsening in the one-component model occurs when the interfaces drift and collide, whereas, in our case, the weaker interfaces gradually erode without moving vertically. The mechanisms of layering are also fundamentally different; the layer dynamics in our model is controlled by the flux ratio of diffusing substances, which has no direct counterpart in the one-component turbulence theory.

Support of the National Science Foundation is gratefully acknowledged. The author thanks Ray Schmitt, Melvin Stern and George Veronis for helpful comments.

REFERENCES

Balmforth, N. J., Llewellyn Smith, S. G. & Young, W. R. 1998 Dynamics of interfaces and layers in a stratified turbulent fluid. *J. Fluid Mech.* **355**, 329–358.

Griffiths, R. W. & Ruddick, B. R. 1980 Accurate fluxes across a salt-sugar finger interface deduced from direct density measurements. *J. Fluid Mech.* **99**, 85–95.

Huppert, H. E. 1971 On the stability of a series of double-diffusive layers. *Deep-Sea Res.* **18**, 1005–1021.

Krishnamurti, R. 2003 Double-diffusive transport in laboratory thermohaline staircases. *J. Fluid Mech.* **483**, 287–314.

Kunze, E. 2003 A review of oceanic salt-fingering theory. *Prog. Oceanogr.* **56**, 399–417.

Lambert, R. B. & Demenkow, J. W. 1972 On the vertical transport due to fingers in double diffusive convection. *J. Fluid. Mech.* **54**, 627–640.

McDougall, T. J. 1991 Interfacial advection in the thermohaline staircase east of Barbados. *Deep-Sea Res.* **38**, 357–370.

Merryfield, W. J. 2000 Origin of thermohaline staircases. *J. Phys. Oceanogr.* **30**, 1046–1068.

Radko, T. & Stern, M. E. 1999 Salt fingers in three dimensions. *J. Mar. Res.* **57**, 471–502.

Radko, T. & Stern, M. E. 2000 Finite amplitude salt fingers in a vertically bounded layer. *J. Fluid Mech.* **425**, 133–160.

St Laurent, L. & Schmitt, R. W. 1999 The contribution of salt fingers to vertical mixing in the North Atlantic tracer release experiment. *J. Phys. Oceanogr.* **29**, 1404–1424.

Schmitt, R. W. 1979 The growth rate of super-critical salt fingers. *Deep-Sea Res.* **26A**, 23–40.

Schmitt, R. W. 1981 Form of the temperature-salinity relationship in the Central Water: evidence for double-diffusive mixing. *J. Phys. Oceanogr.* **11**, 1015–1026.

Schmitt, R. W. 1994 Double diffusion in oceanography. *Annu. Rev. Fluid Mech.* **26**, 255–285.

Stern, M. E. 1969 Collective instability of salt fingers. *J. Fluid Mech.* **35**, 209–218.

Stern, M. E. & Radko, T. 1998 The salt finger amplitude in unbounded T-S gradient layers. *J. Mar. Res.* **56**, 157–196.

Stern, M. E., Radko, T. & Simeonov, J. 2001 3D salt fingers in an unbounded thermocline with application to the Central Ocean. *J. Mar. Res.* **59**, 355–390.

Stern, M. E. & Turner, J. S. 1969 Salt fingers and convective layers. *Deep-Sea Res.* **16**, 497–511.

Turner, J. S. 1967 Salt fingers across a density interface. *Deep-Sea Res.* **14**, 499–611.

Walsh, D. & Ruddick, B. R. 1995 An investigation of Kunze's salt finger flux laws – are they stable? In *Double-Diffusive Convection* (ed. A. Brandt & J. Fernando), pp. 195–211. AGU.

Walsh, D. & Ruddick, B. R. 2000 Double-diffusive interleaving in the presence of turbulence: the effect of a nonconstant flux ratio. *J. Phys. Oceanogr.* **30**, 2231–2245.

Wells, M. G. & Griffiths, R. W. 2002 Localized stirring in a field of salt fingers. *Dyn. Atmos. Oceans* **35**, 327–350.